Medial axis: an application to selective laser manufacturing

Manuel dos Santos Acácio Nhangumbe

Medial axis: an application to selective laser manufacturing

Manuel dos Santos Acácio Nhangumbe

Dissertation to obatain a degree of **Master in Mathematics**

Area of specialization in **Statistics, Optimization and Financial Mathematics**

Jury

President:	José Luís Esteves dos Santos
Supervisors:	Ercília Cristina da Costa e Sousa
	João Eduardo da Silveira Gouveia
Members:	António Manuel Freitas Gomes Cunha Salgueiro
	João Eduardo da Silveira Gouveia

March 3, 2017

Resumo

Fusão seletiva a laser, que é baseada no princípio de fabricação de objetos por adição sucessiva do material, é reconhecida como uma tecnologia de fabrico muito promissora. Esta tecnologia é adequada para o fabrico de objetos com elevada complexidade geométrica que seria impossível por outras formas. Esta tecnologia tem um ponto fraco relacionado com o acabamento superficial, portanto, há uma necessidade de fresar-se o objeto para a remoção do excesso do material ou seja a rugosidade. Para o efeito e com o objetivo de otimizar as sucessivas fases aditivas e subtrativas, propusemos o uso do eixo médio e suas extensões como uma forma prática de resolver o problema e obter um ótimo acabamento superficial. A noção do eixo médio está relacionada com a teoria dos diagramas de Voronoi e já foi proposto em diversos processos de fresagem. É neste contexto que precisamos encontrar a melhor técnica que melhor se adequa à nossa situação para determinar exata ou aproximadamente o eixo médio.

Palavras Chave: Fusão selectiva a laser, diagram de Voronoi, eixo médio, eixo médio truncado, fresagem

Abstract

Selective laser melting, which is based on the principle of material incremental manufacturing, has been recognised as a promising additive manufacturing technology. The technology is suited for creating geometrically complex components that can not possibly or feasibly be made by any other means. Since this technique has a weak point related to the surface finishing, there is a need to use techniques such as milling to remove the surplus material. To plan and optimize the successive additive and subtractive phases, we propose to use the medial axis and certain extensions of it, as a practical way of determining the best possible finishing quality of the produced object. The notion of medial axis is closely related to the theory of Voronoi diagrams, and has been proposed in several milling applications that involve motion planning. To that end we have to find which of the available construction strategies best suits our needs to determine exactly or approximately the medial axis.

Keywords: Selective Laser Melting, Voronoi diagrams, medial axis, truncated medial axis, milling

Acknowledgment

I am very delighted to have reached this moment in my career and it gives me an unmeasurable pleasure to devote my special gratitude to my supervisors Ercília Cristina da Costa e Sousa and João Eduardo da Silveira Gouveia, both PhD in Mathematics, for their dedication, teachings and patience along the work. They turned the hard times into memories, encouraged me to stand tall and work and they put their trust on me. I really appreciate how they made it, thus I take this seldom opportunity to say thank you.

Moreover, I would like to address my greatest thanks to my colleagues, friends and all who were positive to make this project becomes true.

This work is co-financed by the project HEST of Institudo de Bolsas de Moçambique and by the project PT2020-POCI-SII& DT 3414: additive.MILLING - Add Milling to Additive Manufacturing. Co-financed by FEDER (Fundo Europeu de Desenvolvimento Regional), in the scope of the Program Portugal 2020, through COMPETE 2020 (Programa Operacional Competitividade e Internacionalização)

Cofinanciado por:

UNIÃO EUROPEIA
Fundo Europeu
de Desenvolvimento Regional

Contents

Chapter 1

Introduction

The emergence of new technologies in different scientific areas has been boosting and deeply changing the industrial world. Globalization and associated demand have been exposing the industry to a very competitive market. The clients are increasingly demanding and selective, which compels the industry to seriously invest in high-end technologies in order to be more efficient, economically sustainable and to be able to satisfy its clients. In recent years the mould industry has been investing in new technologies, such as Fused Deposition Modeling (FDM), Selective Laser Sintering (SLS), Electron Beam Melting (EBM), Selective Laser Melting (SLM). Their differences are essentially in mechanical details (for more details about these technologies see [31]).

In this work we are concerned with the SLM technology which is nowadays considered one of the most important technologies for metal processing. It is an additive manufacturing technique that uses digital information to produce a 3D metallic object with a *laser* from a metal powder. This technique is characterized by a successive addition of material to a specific area, layer by layer, in opposition to what happens in the traditional manufacturing. In the last years there has been an increasing interest in the use of this technique, mainly because it offers a relative freedom in the geometry of the objects to be manufactured, giving the possibility of producing objects that would be difficult or even impossible to produce using other techniques (see Figure 1.1). Furthermore, the fact that the SLM technology produces objects with high geometric complexity, gives more possibilities to produce personalized objects, with low volume or even economically inviable with convectional manufacturing.

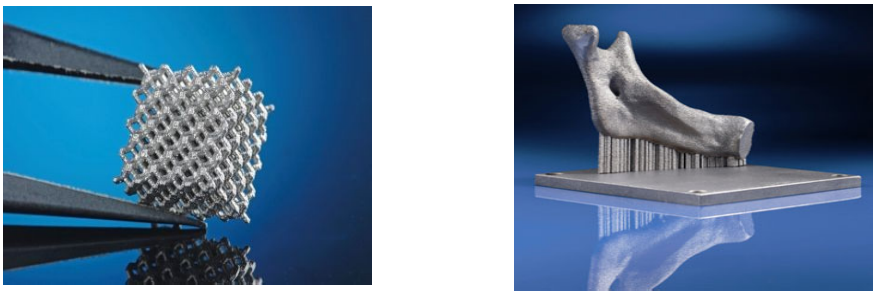

Figure 1.1: Objects produced with SLM technology.

Usually a machine of SLM technology has a computer interface that gives to the operator the possibility of taking control of the production process inside the machine (in Figure 1.2 is shown a machine of SLM technology). To use the SLM technology, it is compulsory to have first a 3D digital model of the object to be produced. The object is then vertically produced regarding a choice of z axis, layer by layer, and therefore it is necessary to know the geometry of each layer, in particular, its contour.

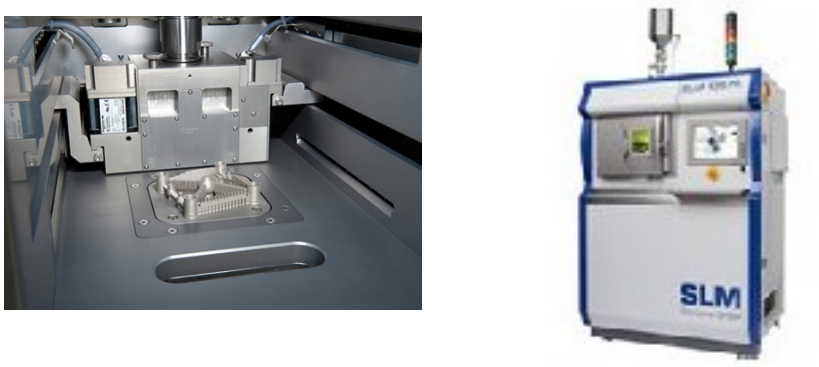

(a) Chamber of the machine (b) SLM Machine

Figure 1.2: Machine of SLM technology and the chamber where the objects are produced.

Assume that a figure is given in three dimensions in the x, y, z axes, where the z axis is the height. Let us cut the figure with the planes $z = z_n,\ z_n \geq 0$. We call *slice* to each layer between $z = z_n$ and $z = z_{n+1}$. In Figure 1.4 we display sections of the object shown in Figure 1.3. The idea is to build the object slice by slice with the thickness of each slice being a parameter of the additive process. The thickness is usually small enough so that the slices can be considered flat for practical geometric purposes.

Figure 1.3: An example of an object to be produced with SLM technology. This is a nose and due to its geometry it is expected to be difficult to produce such object.

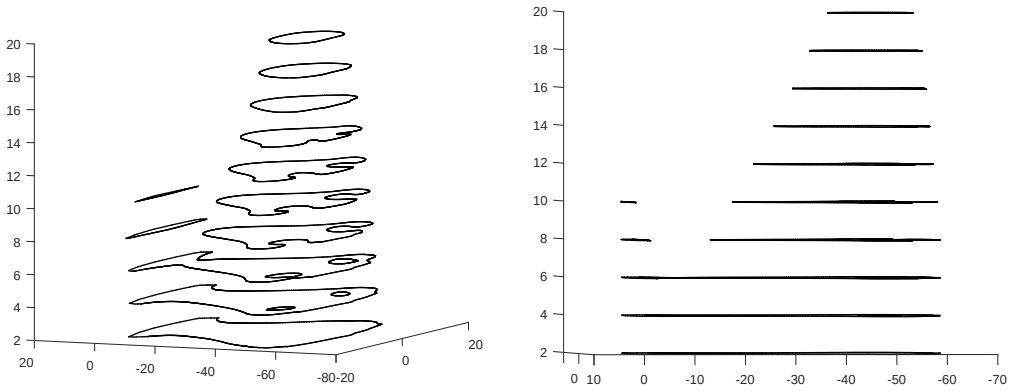

Figure 1.4: Sections related to the object shown in Figure 1.3.

One of the limitations of this technology is related with the efficiency in surface finishing. For that reason, some objects need to be machined to remove the roughness. Therefore, after a first phase of the production it is often applied a second phase that consists in a subtractive process. It is in this context that the industry is searching to bring together both processes, additive and subtractive, to be executed in just one process step by step, or layer by layer.

The additive process gives the desired form to the object, see an example in Figure 1.6, and then the subtractive process removes the surplus material as shown in Figure 1.5.

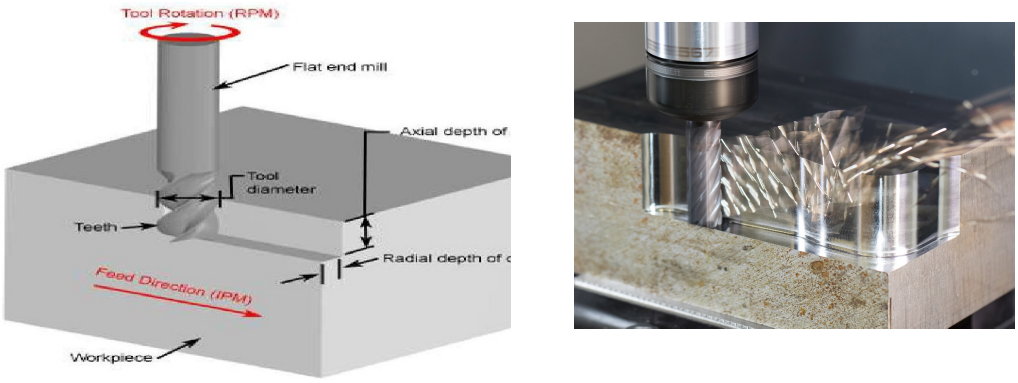

Figure 1.5: Subtractive process. It is necessary to machine a cube to construct the contours that give the form to the object to be designed.

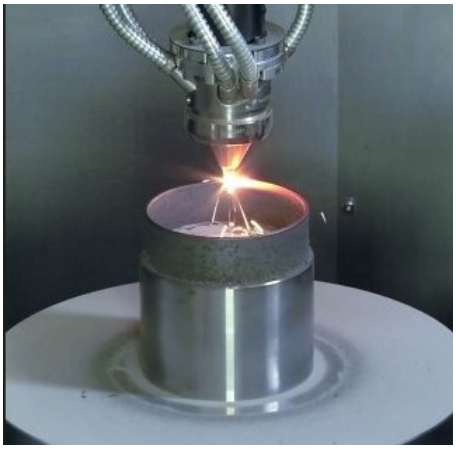

Figure 1.6: Production of an object by the additive process. In contrast to subtractive process, it gives form to the object in the first time it is produced.

One should notice that the surface finishing of an object is an important issue, because it can influence the cost of production. Many mistakes that sometimes culminate in high costs, are due to the need of the surface finishing process. The main goal of this work is to use mathematical tools to construct algorithms that will help us control part of the production process.

The milling cutters have a fixed length and thickness, and if the object has deep cavities it may not be easy to mill the deepest regions after the fabrication is complete. To avoid this problem, one solution is to interrupt the additive process while it is still possible to reach such regions with the milling cutters. After the partial object has been milled, it returns to the additive process from the last quota where it was interrupted. These interruptions are expensive and time-consuming and therefore it is important to decide how many interruptions we need and when

should we have them, in order to minimize the costs.

We assume that the object is given in STL format, and this kind of files stores the geometry of the surface as a set of connected triangles. Therefore the contour of each section is polygonal. More details about these files and its slicing can be found in [11]. For a milling cutter to machine a section two things need to be taken into consideration: the length of the milling cutter must be sufficiently long to reach the section in question, and the diameter sufficiently small in order that the disk defined by the horizontal section of the milling cutter can approximately cover all the points in the polygon. Here, we assume that the milling cutter is cylindrical, therefore its sections are disks. The covered region will be called reachable region or area.

In the next chapters we discuss the theory that is useful to determine or approximate the area in a polygon that can be reached by the milling cutters of a fixed radius. More precisely, in Chapter 2 we introduce the theory of Voronoi diagrams for a finite number of points in the plane and discuss some of its properties and algorithms for its computation. In Chapter 3 we generalize the Voronoi theory to a finite set of bounded objects. We discuss the theory of the medial axis of a planar object and its relationship with the Voronoi diagrams. We also introduce the concept of truncated medial axis that will be the main tool to determine the reachable region in a polygon and then we present some algorithms for the medial axis and truncated medial axis computations. Finally, in the last chapter we talk about the application of the theory presented throughout this work to the original problem and reach some conclusions.

Chapter 2

Voronoi Diagrams

In this chapter we introduce a mathematical theory that will help solve the problem of covering a polygon with circles (disks) of some fixed radius. This theory is based on Voronoi diagrams. The theory of Voronoi diagrams is not a new tool and it has been applied in many different areas, for example, in Biology it has been used for developing an algorithm for the rapid, fully automated location and characterization of molecular channels, tunnels, and pores [24]. And in demographics it is used to test wether more homogenous exposure areas can be generated to reduce ecological bias [15]. We start with an introduction on Voronoi diagrams by giving its definition and some properties. Then, we discuss the construction of the Voronoi diagrams and some applications.

2.1. Definitions and properties

Given a set of points in the plane, that we call sites, the Voronoi diagram is a subdivision of the plane in polygonal regions. Each site is associated to exactly one region. Each region is the locus of points in the plane that are closer to this site than to any other site. An example can be seen in Figure 2.1. Let us first define the Voronoi region.

Definition 2.1. *Let $P = \{p_1, p_2, \ldots, p_n\}$ with $n \geq 2$, be a set of points in $\mathbb{R}^2$, called sites. The Voronoi region $\mathcal{V}(p_i)$ of a site $p_i \in P$ is given by*

$$\mathcal{V}(p_i) = \{x \in \mathbb{R}^2 \ : \ dist(x, p_i) \leq dist(x, p_j), \ j = 1, \ldots, n\}.$$

The Voronoi regions can be defined in high dimensions and with other norms, but the most usually studied case is the planar one with the euclidian norm.

Lemma 2.1. *A Voronoi region is polygonal.*

Proof. We can characterize a Voronoi region through a semi-plane intersection process. Let p_i and p_j be two sites of P and $h(p_i, p_j)$ the semi-plane defined by the

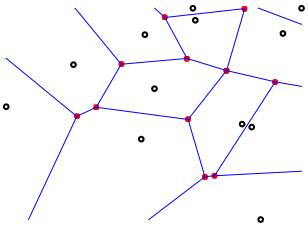

Figure 2.1: Planar Voronoi diagram with 12 sites. The red points are vertices or Voronoi nodes.

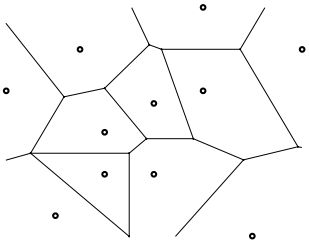

Figure 2.2: Degenerate Voronoi diagram because there exists a node that is an intersection of more than three edges.

bisector of the straight line segment joining these two sites and that contains p_i. Thus, the region $\mathcal{V}(p_i) = \bigcap_{p_j \in P \setminus \{p_i\}} h(p_i, p_j)$ is a polygon. □

The vertices of a Voronoi region are called *Voronoi nodes or Voronoi vertices* and its segments are called *Voronoi edges*. An edge is always on a bisector of two sites and, therefore, the points on an edge are always equidistant to two points of P. In Figure 2.1 the blue lines are Voronoi edges and the red points are Voronoi nodes. We will call Voronoi diagram to the union of Voronoi edges and nodes. The Voronoi diagram of the set P is denoted by $\mathcal{V}(P)$.

Some properties of the Voronoi diagram are presented in this section. The proofs are based on the bibliographic references [22, 23, 25, 29]. In most cases, each node belongs to three edges. However, in some cases, as depicted in Figure 2.2, a node can belong to more than three Voronoi edges. To ensure that each node belongs to exactly three edges we consider the following hypothesis.

Hypothesis 2.1. *In P there are no four co-circular points.*

Each Voronoi region has one site p_i that defines it and this site belongs to this region. Thus, every point $p_i \in P$ has a nonempty Voronoi region. The semi-plane $h(p_i, p_j)$ contains the region $\mathcal{V}(p_i)$ and the semi-plane $h(p_j, p_i)$ contains the region

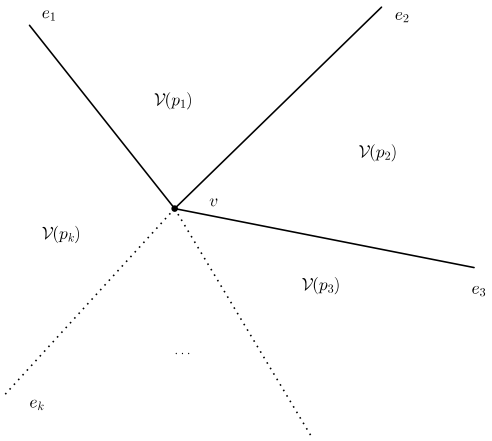

Figure 2.3: Voronoi edges incident to a Voronoi node v.

$\mathcal{V}(p_j)$. The intersection of these semi-plans is just a line. Hence, we can surely state that the interiors of the Voronoi regions of two distinct sites are disjoint. An edge always belongs to two Voronoi regions and it separates the regions of two neighbor points.

Theorem 2.1. *If the hypothesis 2.1 holds, then every Voronoi node is an intersection of exactly three edges and it is equidistant to the three sites of Voronoi regions for which it belongs.*

Proof. A node is an intersection of a set of edges. Let $e_1, e_2, \ldots, e_k$, for $k \geq 2$, be a sequence of edges incident in a node v given clockwise as shown in Figure 2.3. The edge e_i is an intersection of the polygons $\mathcal{V}(p_{i-1})$ and $\mathcal{V}(p_i)$ for $i = 2, 3, \ldots, k$ and e_1 is common to $\mathcal{V}(p_k)$ and $\mathcal{V}(p_1)$. By definition of Voronoi diagram, the node v is equidistant to p_{i-1} and p_i because it belongs to the edge e_i. By the same reason, v is equidistant to p_i and p_{i+1}, and so on. Therefore, v is equidistant to $p_1,\ p_2, \ldots, p_k$. This means that $p_1,\ p_2, \ldots, p_k$ are co-circular, which contradicts our hypothesis when $k \geq 4$. Hence, we have $k \leq 3$.

Now suppose that $k = 2$, then e_1 is common to $\mathcal{V}(p_2)$ and $\mathcal{V}(p_1)$, and so is e_2. These two edges belong to the bisector of the segment $\overline{p_1 p_2}$, which means that they do not intersect the node v, and that is a contradiction. Hence $k = 3$. □

Theorem 2.2. *The polygon $\mathcal{V}(p_i)$ is unbounded if and only if p_i is a boundary point for the convex hull of the set P.*

Proof. If p_i is in the interior of the convex hull of P, then it belongs to the interior of the triangle $p_1 p_2 p_3$, with p_1, p_2, p_3 in P. Let us consider the circles C_{12}, C_{23} and

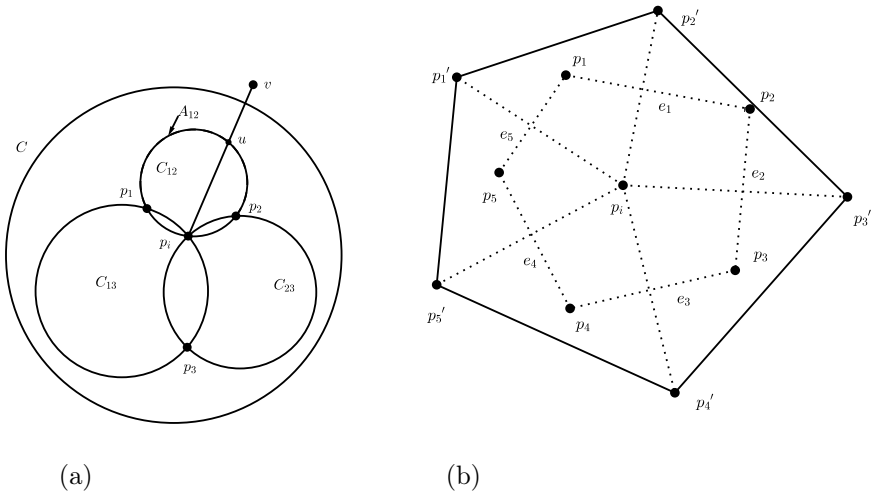

Figure 2.4: Illustration of the proof of Threorem 2.2.

C_{13} with finite radius passing through the point p_i and through the pairs $\{p_1, p_2\}$, $\{p_2, p_3\}$ and $\{p_1, p_3\}$, respectively (see Figure 2.4a). The arc A_{12} is the one between p_1 and p_2 that does not contain p_i. Similarly, we define the arcs A_{23} and A_{13}. Any point of A_{12} is closer to p_1 or p_2 than to p_i. Let C be a circle that contains C_{12}, C_{23} and C_{13}. We are going to show that any point v outside C is closer to p_1, p_2 and p_3 than to p_i. The segment $\overline{vp_i}$ intercepts one of the sides of the triangle $p_1p_2p_3$. Let such side be $\overline{p_1p_2}$, then this segment also intercepts the arc A_{12} at point u. Either p_1 or p_2 are closer to u than p_i, since it belong to the shorter up_i arc.

Let u be closer to p_2, then $dist(p_i, u) + dist(u, v) \geq dist(p_2, u) + dist(u, v)$. By the triangular inequality we get $dist(p_2, u) + dist(u, v) \geq dist(p_2, v)$ which means that v is closer to p_2 than to p_i. Hence, any point v outside the circle C is closer to p_1, p_2 or p_3 than to p_i. Thereby, the polygon $\mathcal{V}(p_i)$ is contained in the circle C, and consequently it is bounded. Conversely, we suppose that the polygon $\mathcal{V}(p_i)$ is bounded and let $e_1, e_2, \ldots, e_k$, $k \geq 3$ be the sequence of edges of the boundary. Each edge e_k belongs to a bisector of the segment $\overline{p_ip'_h}$, $p'_h \in P$ (see Figure 2.4b). It can be seen that p_i is in the interior of the polygon $p'_1p'_2 \cdots p'_k$ which means it is not a boundary point for the convex hull of P. □

Since only unbounded polygons can have rays as edges, the rays of the Voronoi diagram correspond to pairs of adjacent points of P on the convex hull. Next, we consider the dual of the Voronoi diagram, i.e., the graph with vertex set P and edges joining the sites of P whose Voronoi polygons share an edge. Each Voronoi edge corresponds to an edge in the dual graph that is called dual edge (see the Figure

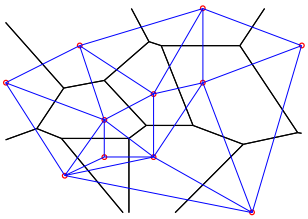

Figure 2.5: Delaunay triangulation and its vertices.

2.5).

Theorem 2.3. *If we assume Hypothesis 2.1, then the dual graph of the Voronoi diagram is a triangulation of P and is called the Delaunay triangulation denoted by $\mathcal{D}(P)$.*

Proof. Immediate consequence of the Theorems 2.1 and 2.2. □

In Figure 2.5 the Voronoi diagram is displayed in black and the associate Delaunay triangulation is in blue. The points highlighted in red are sites, that is, are vertices of the Delaunay triangulation.

Lemma 2.2. *Assuming Hypothesis 2.1, the Voronoi diagram of n sites has at most $2n-5$ nodes and $3n-6$ edges. The Delaunay triangulation of n sites has at most $3n-6$ edges and $2n-4$ faces.*

Proof. Each dual edge corresponds to a unique edge in the Voronoi diagram and by Theorem 2.3 it is a triangulation. Therefore, the Delaunay triangulation is a planar graph of n vertices. Let us consider the Euler's formula for a planar graph

$$n_v - n_a + n_f = 2, \tag{2.1}$$

where n_v, n_a, n_f denote the number of vertices, edges and faces, respectively.

In this case $n_v = n$. If we count the number of edges in the Delaunay triangulation using the faces we get a maximum of $3n_f$ edges, because each triangle comprises three edges. On the other hand, since each edge is shared by two triangles the edges are counted twice, that is, we obtain the inequality $\frac{3n_f}{2} \leq n_a$. Substituting into the Euler's formula it is easily seen that $n_a \leq 3n-6$ e $n_f \leq 2n-4$.

Thus we can state that the Delaunay triangulation has a maximum of $3n-6$ and $2n-4$ faces and hence the number of Voronoi edges is at most $3n-6$. Each face of the Delaunay triangulation dualizes to a Voronoi node and vice-versa. However,

there exists an unbounded face in the Delaunay triangulation that do not dualize. Hence we have at most $2n - 5$ nodes. □

The number of edges for each Voronoi region depends on the way the sites are distributed. A Voronoi polygon (region) has at most $n - 1$ edges. Since the Voronoi diagram has n polygons and at most $3n - 6$ edges, where each edge is shared by exactly two polygons then the average is at most six. For more details about the calculation of the average see [9, 10].

2.2. Construction of the Voronoi Diagram

Before discussing the construction of the Voronoi diagram, we discuss the idea of the algorithm *divide and conquer*. The essence of this algorithm is to split a given problem into two subproblems approximately equal and solve them recursively. At the end, the solutions are joined together to get just one solution for the original problem. Generally, the reduction of the original problem to two subproblems is simple but the step of concatenating the solutions is more demanding and tricky. Preparata and Hong [26] were the first to apply the divide and conquer technique to the problem of finding the convex hull of a given number of points.

We now introduce the following definition that will be necessary for the theorems throughout the text.

Definition 2.2. *Let $f(n)$ and $g(n)$ be two numerical sequences. It is said that $f(n) = \mathcal{O}(g(n))$ if exists a constant $M > 0$ such that*

$$f(n) \leq Mg(n),\ n \to \infty.$$

If $g(n) = n^k$ we say that $f(n)$ is of order k. In particular if $k = 1$, $f(n)$ is said to be linear.

Now, we need to assume the following:

Hypothesis 2.2. *There are no three collinear points or two points on a vertical line.*

In this case we can construct the following algorithm for finding a convex hull of a finite number of points, in $\mathbb{R}^2$.

Algorithm 2.1 (Convex hull)**.**
Input: A finite set P.
Output: The convex hull $\mathcal{H}(P)$.
Steps:

1. *Organize the points in ascending order relative to the coordinate x;*
2. *Split the set P of points into two sets P_1 and P_2, each one containing half of the points;*
3. *Find the convex hull $\mathcal{H}(P_1)$ of P_1 and $\mathcal{H}(P_2)$ of P_2 recursively;*
4. *Combine $\mathcal{H}(P_1)$ and $\mathcal{H}(P_2)$ in order to obtain $\mathcal{H}(P_1 \cup P_2)$.*

The step 1 ensures that the sets P_1 and P_2 are separated by a vertical line and there is no superposition of points. This step simplifies the step 4. The steps 2, 3 and 4 are repeated recursively until $n \leq 3$. If $n = 3$, the convex hull is a triangle by the assumption of non collinearity. The major difficulty is on step 4. Suppose that the convex hulls are $H_1 = \mathcal{H}(P_1)$ and $H_2 = \mathcal{H}(P_2)$. Then $\mathcal{H}(P_1 \cup P_2) = \mathcal{H}(H_1 \cup H_2)$. We want to find two tangent lines to both hulls located on the upper and bottom parts. Let T be a line segment that connects the rightmost point of H_1 and the leftmost point of H_2. We move downward the extremities of the segment T in an alternating way, first on one hull and then on the other until the bottom tangent is reached (see Figure 2.6). The upper tangent is obtained similarly, thus we take in total a linear time $\mathcal{O}(n)$ to determine the convex hull of the two sets.

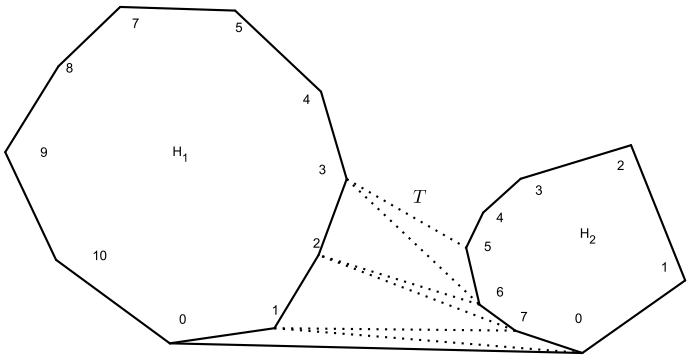

Figure 2.6: Illustration of how to find the bottom tangent line of two convex hulls.

Thus we have the following result.

Theorem 2.4. *The divide and conquer algorithm for the convex hull of n points takes at most $\mathcal{O}(n \log n)$ time.*

Proof. The binary tree of the algorithm has $\mathcal{O}(\log_2 n)$ levels each taking $\mathcal{O}(n)$ time. □

Now, let us consider the divide and conquer algorithm to construct the Voronoi diagram for n sites. Let $P = \{p_1, p_2, \ldots, p_n\}$ be the set of sites, we call it *generator set*. We assume that the elements of P are in ascending order regarding the x axis and that the Hypotheses 2.1 and 2.2 hold.

Algorithm 2.2 (Divide and conquer method)**.**
Input: The generator P with its points in ascending order.
Output: Voronoi diagram for P.
Steps:

1. *If $n \leq 3$, then construct the Voronoi diagram directly and go to step 3.*
2. *Else do:*
   (a) *Split P into two subsets with half of the points, P_E left half and P_D right half.*
   (b) *Construct the Voronoi diagrams $\mathcal{V}_E = \mathcal{V}(P_E)$ and $\mathcal{V}_D = \mathcal{V}(P_D)$.*
   (c) *Concatenate $\mathcal{V}(P_E)$ and $\mathcal{V}(P_D)$ and obtain a unique Voronoi diagram $\mathcal{V}$ of P.*
3. *Return $\mathcal{V}(P)$.*

As in the convex hull computation, we need to pay special attention to the concatenating step.

Algorithm 2.3 (Concatenating two Voronoi diagrams)**.**
Input: The Voronoi diagrams $\mathcal{V}_E$ e $\mathcal{V}_D$.
Output: Voronoi diagram $\mathcal{V} = \mathcal{V}_E \cup \mathcal{V}_D$.
Steps:

1. *Construct the convex hulls H_E and H_D of P_E and P_D, respectively.*
2. *Find the common bottom holder (bottom tangent line) of H_E and H_D, denoted $I(P_E, P_D)$ and let $b(p_E, p_D)$ be the bisector of the bottom holder.*
3. *Define w_0 as the point at infinity on the ray $b(p_E, p_D)$, and $i \leftarrow 0$.*
4. *While $I(P_E, P_D)$ is not superior (upper), repeat the following:*
   (a) $i \leftarrow i + 1$.

(b) *Find a point* a_E *(different from* w_{i-1}*) that is an intersection of* $b(p_E, p_D)$ *with the boundary of* $\mathcal{V}(p_E)$.

(c) *Find a point* a_D *(different from* w_{i-1}*) that is an intersection of* $b(p_E, p_D)$ *with the boundary of* $\mathcal{V}(p_D)$.

(d) *If* a_E *has its ordinate less than* a_D *then,*
$w_i \leftarrow a_E$ *and*
$p_E \leftarrow$ *the generator on the other side of the Voronoi edge that contains* a_E
else $w_i \leftarrow a_D$ *and*
$p_D \leftarrow$ *the generator on the other side of the Voronoi edge that contains* a_D.

5. $m \leftarrow i$.
$w_{m+1} \leftarrow$ *a point in the upper infinity of* $b(p_E, p_D)$.

6. *Add the polygonal line* $(\overline{w_0w_1}, \overline{w_1w_2}, \ldots, \overline{w_mw_{m+1}})$, *and erase from* $\mathcal{V}_E$ *and* $\mathcal{V}_D$ *the unnecessary lines on the right and left sides of the polygonal line. Return the Voronoi diagram.*

The Figures 2.7 and 2.8 depict the execution of the Algorithm 2.3.

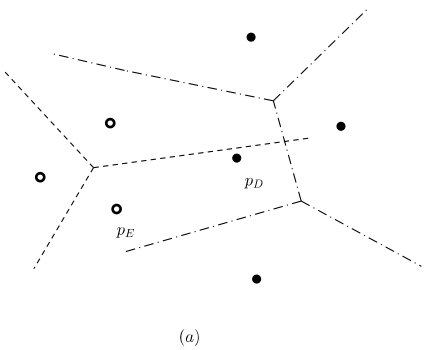

(a)

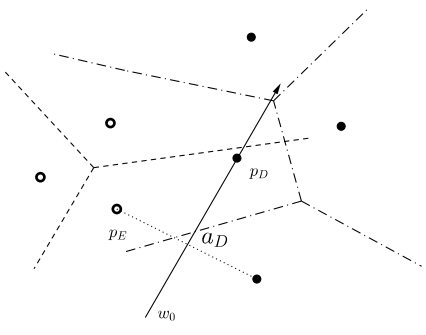

(b)

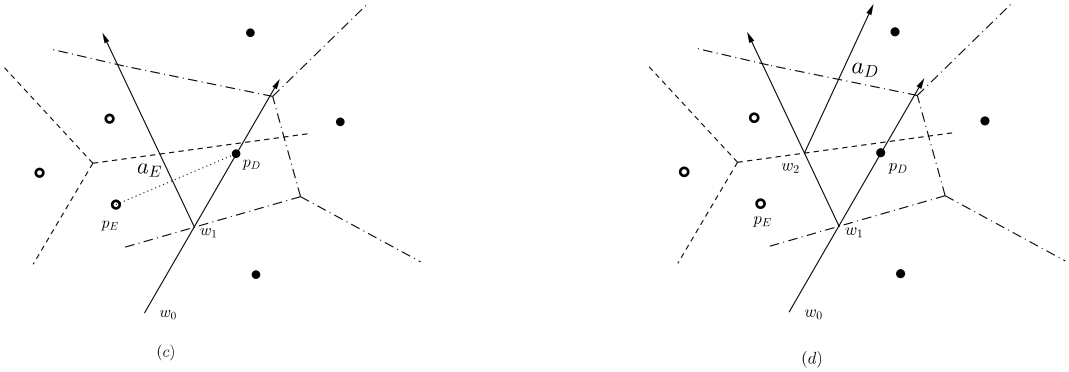

Figure 2.7: Concatenation of Voronoi digrams. In (a) are shown two Voronoi diagrams to be joined together and (b), (c) and (d) show the following iterations when the concatenating algorithm is applied.

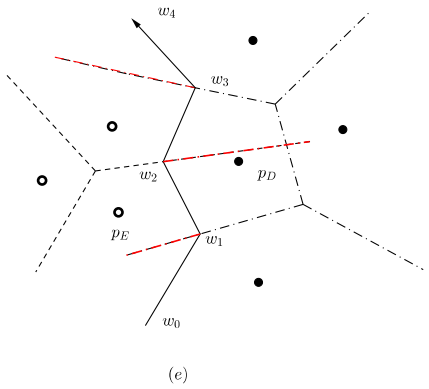

Figure 2.8: Concatenation of Voronoi digrams. In this diagram the construction lines highlighted in red must be erased to obtain the desired diagram.

Theorem 2.5. *The divide and conquer algorithm takes an optimal time of* $\mathcal{O}(n \log n)$ *to construct a Voronoi diagram* $\mathcal{V}(P)$ *of* P *with* n *sites.*

Proof. The proof is similar to the previous theorem. □

2.3. Largest empty circle

Consider the problem of *the largest empty circle*, that is, we want to find the largest empty circle whose center is in the convex hull $\mathcal{H}(P)$, given n sites. A circle is said to be empty if it contains no site in its interior and is said to be largest if there is no other empty circle with strictly larger radius.

Let $f(p)$ be the function defined as the radius of the largest empty circle centered on p where p is any point in the plane inside $\mathcal{H}(P)$. We want to find a maximum

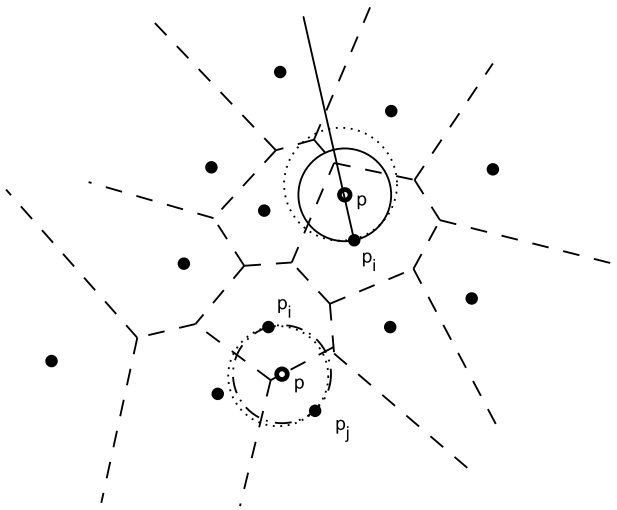

Figure 2.9: Center p inside the convex hull.

for this function regarding the variable p in the convex hull of P. Seemingly, there exist an infinite number of candidate points to be a maximum, but making use of Voronoi diagrams we will turn this infinity into a finite number and in this way we can efficiently solve the problem.

Let p be a point that is in the interior of the convex hull $\mathcal{H}(P)$. Suppose that we inflate a circle from p in $\mathcal{H}(P)$, the circle of largest radius that contains a site of P is the circle of radius $f(p)$. If at the radius $f(p)$ the circle contains just one site p_i then $f(p)$ can not be a maximum of the radius function. Notice that moving the point p a way from p to p' along the radius $\overline{p_i p}$ we get $f(p')$ that is greater than $f(p)$. Thus, p can not be a local maximizer of f because there exists p' in the neighborhood of p where $f(p')$ takes a larger value (see Figure 2.9).

Next, consider $f(p)$ in a way that exactly two sites p_i and p_j $(i \neq j)$ are contained in the circle. Again $f(p)$ can not be a maximizer because when p is moved to p' along the bisector of $\overline{p_i p_j}$ and away from $\overline{p_i p_j}$ we get that $f(p')$ increases. Hence, only when the circle touches exactly three sites can the radius $f(p)$ be maximum. If the circle includes three sites in a way that they span more than a semicircle (see Figure 2.10) then the translation of p to any direction approaches p to a certain site decreasing the radius $f(p)$, otherwise we could translate it a little and increase $f(p)$. Consequently, we have proven the following lemma.

Lemma 2.3. *If the center p of a largest empty circle is strictly interior to the convex hull $\mathcal{H}(P)$ then it coincides with a Voronoi node.*

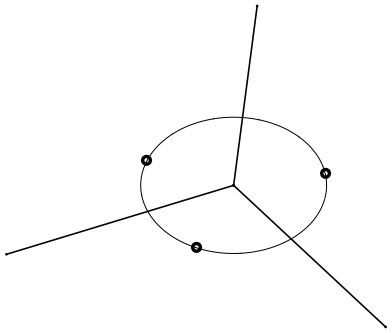

Figure 2.10: The circle with the radius $f(p)$ containing three sites.

Finally, consider the center p on the boundary of $\mathcal{H}(P)$. For this case we are going to use a different argument because moving p towards p' may exit the convex hull. We will use a more intuitive approach. Suppose that $f(p)$ is a maximum with p lying on the boundary of $\mathcal{H}(P)$ and that the circle contains just one site. It is seen that p can not be a vertex of $\mathcal{H}(P)$ because the vertices of $\mathcal{H}(P)$ are sites also, which means that $f(p) = 0$. Thus p is in the interior an edge e_k of $\mathcal{H}(P)$. Therefore, when moving p a long e_k its distance to p' must increase. If the circle centered at p contains two sites p_i and p_j, then it is possible that the direction along the bisector of both sites leads outside the convex hull. Thus, we get that $f(p)$ is a local maximum (see the Figure 2.11). As a consequence the following lemma holds.

Lemma 2.4. *If the center p of the largest empty circle lies on the boundary of the convex hull $\mathcal{H}(P)$, then it lies on a Voronoi edge.*

Considering these last two lemmas, we restrict ourselves to a finite number of candidates. We just look at the Voronoi nodes and the intersections of the boundary of the convex hull of P with the Voronoi edges.

***Observation* 2.1.** *In general:*

- *It is not true that every Voronoi node is a local maximizer of f.*
- *Not all Voronoi nodes need to be inside the convex hull $\mathcal{H}(P)$ of their corresponding sites (see Figure 2.5), therefore it is necessary to check if the node is inside $\mathcal{H}(P)$.*
- *The largest empty circle defined in this section is also called Delaunay disk.*

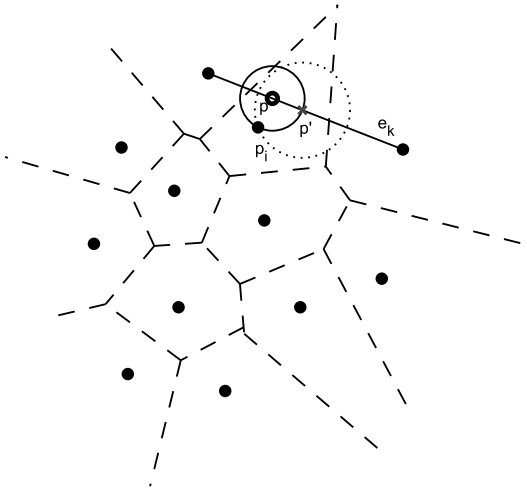

Figure 2.11: The center p on the boundary of the convex hull.

We have obtained an efficient Voronoi theory based algorithm to find the largest empty circle centered in a convex hull of a finite set of points, as quantified in next the result.

Lemma 2.5. *Let $P = \{p_1, p_2, \ldots, p_n\}$ be a set of n points in the plane. The problem of determining the largest empty circle centered inside the convex hull $\mathcal{H}(P)$ can be solved in $\mathcal{O}(n \log n)$ time.*

Chapter 3

Medial axis

In the previous chapter we have introduced the notion of Voronoi diagrams associated to points in the plane. They will play a fundamental rule in the study of another object, the medial axis. To see this, we first introduce the concept of medial axis and then discuss the relation between the medial axis and Voronoi diagrams.

In Section 3.1 we define the medial axis of a planar shape, describe its main features and present some of its applications. Then, in Section 3.2, we generalize the Voronoi theory and discuss its relationship with the medial axis. In Section 3.3 we introduce the concept of truncated medial axis which is going to be the important tool for finding the reachable region for each slice to be milled. Then in Sections 3.4 and 3.5 we discuss exact and approximated algorithms to obtain the medial axis, studying the main theoretical properties.

3.1. Definitions and properties

The medial axis was first introduced by Harry Blum applied to biological shapes in 1967 [5]. Intuitively, the medial axis is often defined using the classical example called *grass fire*. Imagine starting a fire at the same time everywhere on the boundary of a shape in the plane, the fire spreads into the shape at constant speed in every direction. The medial axis is the set of points where the wavefront of the fire meets itself.

Mathematically, the medial axis is the set of all points in the plane that have at least two closest points on the boundary of the shape. The medial axis can be defined in $\mathbb{R}^n$ and thus, it will be of dimension $n-1$. In the plane it is a one dimensional object. We exemplify it in Figure 3.1. The blue line is the medial axis of the shape in which it is enclosed.

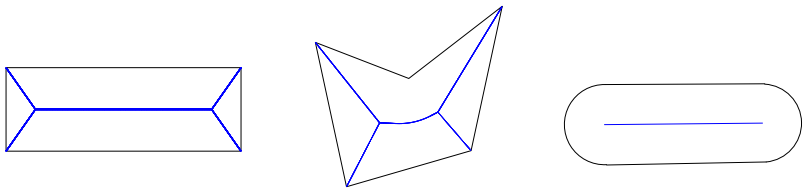

Figure 3.1: The blue line is the medial axis.

There have been many applications for the medial axis. In robotics for motion planning, it is used to find a free path (free in the sense that there is no obstacles in it) to move a point, a circle, a segment or a polygon in the plane [16, 23]. In Solid Modeling the medial axis transform is helpful to generate 3D polyhedral solids of arbitrary genus without cavities. In image processing, the medial axis is used for image analysis and mathematical morphology of objects reducing shapes into short caricatures [28]. In Geo-spatial Information System it is a fundamental tool for the evaluation of spatial relationships and it is useful in the extraction of features from digitized or scanned data. Terrain and runoff modeling, especially from contours, can be described using medial axis extraction [12, 33]. The medial axis has been proposed in virtual endoscopy as a tool for automated path planning for this procedure [4]. In general, medial axis extraction is a strong tool in several visual computing applications because it provides a more compact representation of solid models while preserving their topological properties and features.

We are interested in using the medial axis to find a region that can be reached by a milling cutter in a polygon. Before we discuss algorithms we need a solid theory about the medial axes and their main features.

Let us start by defining the Hausdorff distance. Given two sets in the plane, say A and B, the distance from A to B is the Hausdorff distance if

$$d(A, B) = \inf\{||x - y||_2 \ : \ x \in A, y \in B\}. \tag{3.1}$$

If A and B are points then the Hausdorff distance is equivalent to the euclidian one.

Let X be an object in the plane and assume that X is a compact set, connected but not necessarily simply connected and that is equal to the closure of its interior. A set with these characteristics will be called a *compact body.*

Definition 3.1 (Medial axis)**.** *Let X be a compact body. The medial axis of X is the set of points in X that have at least two closest points on the boundary of X and*

we denote it by $M(X)$.

Alternatively, we can attempt to define the medial axis of X using maximal closed disks inside X. A disk $B_r(x) \subseteq X$ is said to be maximal if it is not enclosed in any other disk inside X. Formally, we define the set of centers of maximal disks in X, $B_{max}(X)$, as the set of points x for which there is an $r > 0$ such that for any $x' \in \mathbb{R}^2$ and $r' > 0$, $B_r(x) \subseteq B_{r'}(x') \subseteq X$ implies that $x = x'$ and $r = r'$.

Proposition 3.1. *Let* X *be a compact body in the plane, then*

$$M(X) \subseteq B_{max}(X).$$

Proof. Let $x \in M(X)$. Then there exist $p_1, p_2 \in \partial X$, $p_1 \neq p_2$ such that

$$d(x, p_1) = d(x, p_2) = \min_{p \in \partial X} d(x, p).$$

This means, there is a disk B_r enclosed in X with radius $r = \min_{p \in \partial X} d(x, p)$ centered at x. Each disk in X containing B_r is equal to B_r, i.e. B_r is a maximal disk. Thus, $x \in B_{max}(X)$, which means

$$M(X) \subseteq B_{max}(X).$$

□

Example 3.1. *In this example we show that the medial axis is not topologically a closed line, that is,* $M(X) \neq \overline{M(X)}$. *Consider the ellipse in Figure 3.2. The blue line is the medial axis of this ellipse but it does not contain its endpoints. Each endpoint is a center of an osculating disk touching the ellipse on just one point (vertex of the ellipse) and they are also maximal disks, thus, these endpoints do not belong to the medial axis.*

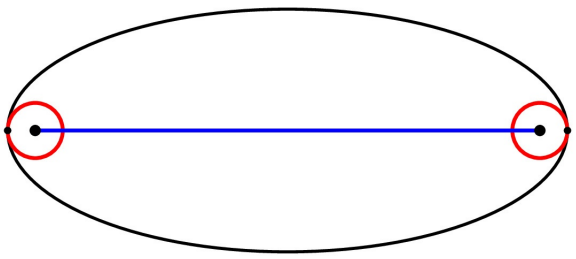

Figure 3.2: The red disks are osculating disks (maximal disks) in the ellipse. Their centers do not belong to the medial axis (blue line) because they touch the ellipse on just one point.

Example 3.2. *The set $B_{max}(X)$ does not need to be closed as can easily be seen in a triangle whose medial axis does not contain the vertices. But is the set $B_{max}(X)$ closed relative to the interior of X? The answer is still negative. See Figure 3.3, the limit point B of the triangles does not induce a limit dendrite on the set $B_{max}(X)$.*

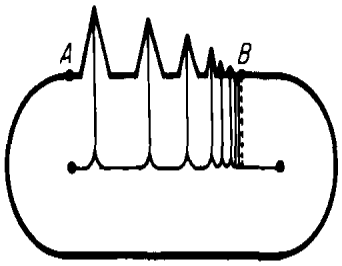

Figure 3.3: The limit point B of the triangles does not induce a limit dendrite on the set $B_{max}(X)$.

Proposition 3.2. *Let X be a polygonal compact body, then*

$$M(X) = B_{max}(X). \tag{3.2}$$

Proof. The inclusion

$$M(X) \subseteq B_{max}(X)$$

follows directly from the Proposition 3.1. Now we show that

$$B_{max}(X) \subseteq M(X).$$

Consider $x \in B_{max}(X)$, that is, x is a center of a maximal disk in X. A maximal disk in a polygon touches the boundary on at least two points and the distance $d(x, \partial X)$ is its radius. Furthermore, the radius $d(x, \partial X)$ is minimum because otherwise the disk would not be contained in X, hence $x \in M(X)$ and

$$B_{max}(X) \subseteq M(X).$$

□

The result of Proposition 3.2 is not true for general compact bodies as can be seen in Example 3.1. It can, however still be generalized into the case where X is a compact body if we make suitable adaptations. The following result was proven by G. Matheron [19].

Proposition 3.3. *Let X be a compact body. Then,*

$$\overline{M(X)} = \overline{B_{max}(X)}. \tag{3.3}$$

Let $B_{r_{\max}}(x)$ be the largest disk that is contained in P with center at $x \in M(P)$ and $R(x) = \min_{y \in \partial P} \{||x - y||_2$. $R(x)$ is the radius of the disk $B_{r_{\max}}(x)$.

Theorem 3.1. *Let P be a polygon. Then,*

$$P = \overline{\bigcup_{x \in M(P)} B_{r_{\max}}(x)}. \tag{3.4}$$

Proof. The set of disks in a polygon P containing a given point p in the interior of P is nonempty and partially ordered regarding the inclusion relation. Any chain $\{D_i\}_{i \in I}$ of disks in this partial order, i.e. a collection of disks that is totally ordered, has a supreme, namely, $\bigcup_{i \in I} D_i$ which is a disk. By Zorn's Lemma, any partially ordered set for which all chains have a supreme has a maximal element. This gives us a maximal disk containing p, so the point p is contained in a maximal disk. Since P is the closure of its interior the result follows. □

From this theorem, we conclude that the polygon P can be reconstructed by the union of maximal disks with radius $R(x)$. The medial axis preserves the topology (shape) of the original object in which it is enclosed. If the object is connected the medial axis is also connected and the object has the same number of holes as its medial axis. For more properties and applications of the medial see [8, 21]. In Figures 3.4 some polygons with the corresponding medial axes are shown.

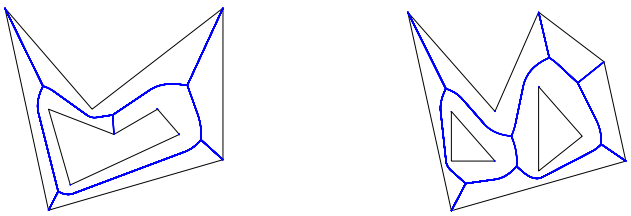

(a) Polygon with one hole (b) Polygon with two holes

Figure 3.4: Medial axes of polygons with holes.

3.2. Generalized Voronoi diagrams

In general, the medial axis is closely related to generalized Voronoi diagrams. We will first give a brief introduction to generalized Voronoi diagrams [17, 18, 30].

The concept of Voronoi diagrams can be generalized in different ways. In this work we will consider that the generator L can be a set comprising bounded objects in the plane, such as, straight line segments, a chain of straight line segments or circles. Let us suppose that $L = \{L_1, \ldots, L_n\} \subseteq \mathbb{R}^2 (1 \leq n < \infty)$ where L_i is a bounded set. We assume that the elements of L do not intercept one another and we define a Voronoi region associated to L_i as

$$\mathcal{VR}(L_i) = \{p \in \mathbb{R}^2 \ : \ d(p, L_i) \leq d(p, L_j), \ i \neq j, j \in I_n = \{1, 2, \ldots, n\}\}. \tag{3.5}$$

If L_i, $i \in I_n$ are all points, it easy to see that $\mathcal{V}(L_i)$ will be exactly the one defined in Section 2.1.

Definition 3.2. *Let $L = \{L_1, L_2, \ldots, L_n\} \in \mathbb{R}^2$ be a generator set. The set $\mathcal{VD}(L) = \bigcup_{i=1}^{n} \partial\mathcal{VR}(L_i)$ is a generalized Voronoi diagram generated by L.*

If $L_i, \ i \in I_n$ are points, we obtain the Voronoi diagram defined in Section 2.1. The Figure 3.5 shows a planar line Voronoi diagram generated by two segments.

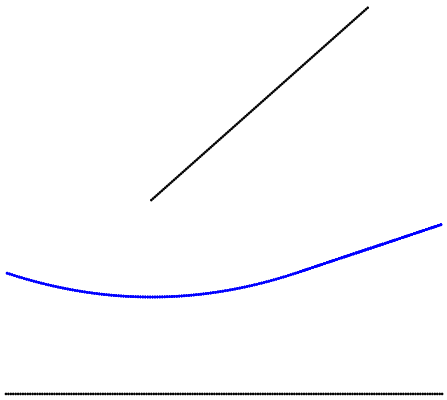

Figure 3.5: The blue line is the Voronoi diagram generated by two segments.

The dominance of L_i over L_j, for $i \neq j, \ i, j \in I_n$ can be defined as

$$Dom(L_i, L_j) = \{p \in \mathbb{R}^2 \ : \ d(p, L_i) \leq d(p, L_j)\}. \tag{3.6}$$

The dominance is a closed region bounded by a bisector that is not necessary a straight line. From the definition of dominance we can conclude that

$$\mathcal{VR}(L_i) = \bigcap_{j \in I_n \setminus \{i\}} Dom(L_i, L_j). \tag{3.7}$$

Also, when L_i are not all points the associated Voronoi regions $\mathcal{V}(L_i)$ are not necessarily convex polygons. Since the boundary ∂P of a polygon P is a chain of straight line segments we can find its Voronoi diagram. We will consider the vertices of a polygon P to be defined as the endpoints of straight line segments constituting its boundary and the edges to be open segments that are obtained by deleting the endpoints of the segments constituting the boundary of P. We consider the generator L comprising the edges and vertices of P, i.e. $L = \{e_i\}$, $i \in I_n$ where e_i is a point or an open segment. Taking the Voronoi diagram of this generator set we will further prune it, considering for any element e_i only the part of its Voronoi region that is contained in P. We get in this way a new diagram, $\mathcal{VD}(P)$, that is said to be the Voronoi diagram of the polygon P. In Figure 3.6 is shown an example of Voronoi diagram of a polygon.

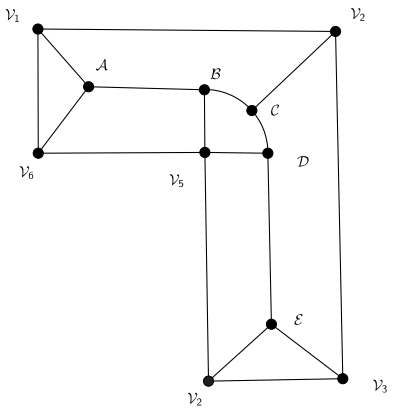

Figure 3.6: The lines inside the polygon $\mathcal{V}_1, \mathcal{V}_2, \mathcal{V}_3, \mathcal{V}_4, \mathcal{V}_5, \mathcal{V}_6$ make its Voronoi diagram.

In the example, the Voronoi region of the open segment $(\mathcal{V}_6, \mathcal{V}_5)$ is the quadrangle $\mathcal{V}_6, \mathcal{A}, \mathcal{B}, \mathcal{V}_5, \mathcal{V}_6$ and the Voronoi region of $\mathcal{V}_5$ is the region $\mathcal{V}_5, \mathcal{B}, \mathcal{C}, \mathcal{D}, \mathcal{V}_5$.

A polygon is called *simple* if it is homeomorphic to a disk. Simple polygons have connected boundaries, particularly, they contain no holes. Each vertex $\mathcal{V}_i$ belongs to an internal angle in the polygon. If the internal angle is convex we say that the *vertex is convex* and we say it is *reflex* otherwise.

Lemma 3.1. *The Voronoi region of a convex vertex is the vertex itself and the Voronoi diagram of a segment or a reflex vertex is a two dimensional set.*

Proof. Consider a polygon given by its elements $\{e_i\}$ where e_i is a vertex or an open segment. We divide the proof into three steps.

First, let e_i be a convex vertex and suppose that $\mathcal{VR}(e_i)$ has other point u in the polygon that is different from e_i. By the triangular inequality any point in the segment $\overline{e_i u}$ must be in $\mathcal{VD}(e_i)$. But a point in that segment sufficiently close to e_i, is closer to the adjacent edges than to e_i itself. That means u must be equal to e_i and $\mathcal{VR}(e_i)$ contains no other point in the polygon different from e_i.

Next, let e_i be a segment. If e_{i-1} and e_{i+1} are the adjacent elements then we consider the bisectors $b(e_{i-1}, e_i)$ and $b(e_i, e_{i+1})$, see Figure 3.7. The planar region bounded by $b(e_{i-1}, e_i)$, $b(e_i, e_{i+1})$ and e_i is a set of points closer to e_i than to e_{i-1} and e_{i+1}. On the other hand, there is a positive distance from e_i to any other non-adjacent site of the polygon and we denote the minimum of these distances by ε. Now we construct a line segment that is parallel to e_i at the distance $\frac{\varepsilon}{2}$ from e_i and with endpoints on the bisectors $b(e_{i-1}, e_i)$, $b(e_i, e_{i+1})$. The set of points bounded by this segment, $b(e_{i-1}, e_i)$, $b(e_i, e_{i+1})$ and e_i is a two dimensional region contained in $\mathcal{VR}(e_i)$, thus $\mathcal{VR}(e_i)$ is also a two dimensional region.

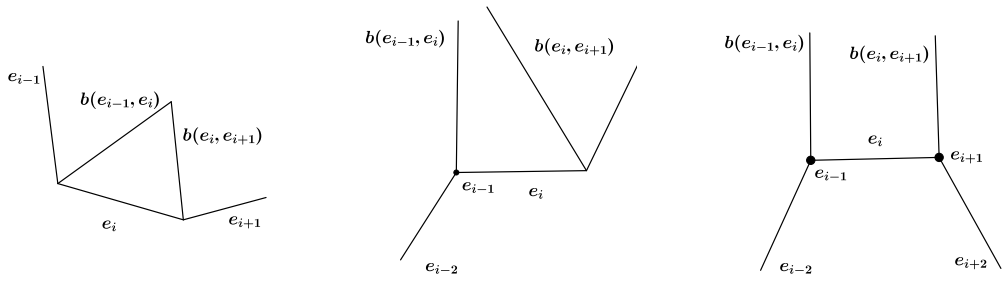

(a) (b) (c)

Figure 3.7: Second case: e_i is an open segment.

Finally, if e_i is a reflex vertex then the bisectors $b(e_{i-1}, e_i)$, $b(e_i, e_{i+1})$ intercept each other on e_i, see Figure 3.8, forming an angle greater than zero. We also know that there is a positive distance from e_i to any other non-adjacent site of the polygon and we denote the minimum of these distances by ε. Now we construct circular arc at the distance $\frac{\varepsilon}{2}$ from e_i and with endpoints on the bisectors $b(e_{i-1}, e_i)$, $b(e_i, e_{i+1})$. The set of points bounded by this arc, $b(e_{i-1}, e_i)$, $b(e_i, e_{i+1})$ and e_i is a two dimensional region contained in $\mathcal{VR}(e_i)$, hence $\mathcal{VR}(e_i)$ is also a two dimensional region.

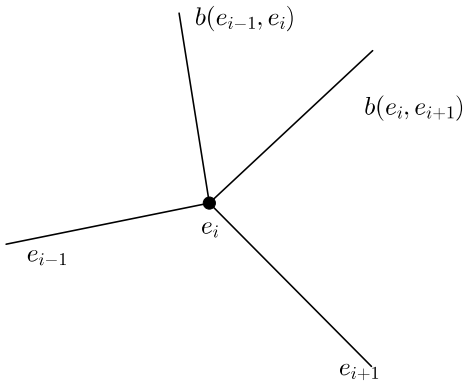

Figure 3.8: Third case: e_i is a reflex vertex.

□

Definition 3.3. *A Voronoi vertex is a point of intersection of at least three Voronoi regions. A segment or curve that belongs to two Voronoi regions and with Voronoi vertices as endpoints will be referred to as Voronoi edge.*

In Figure 3.6 the points $\mathcal{A}, \mathcal{B}, \mathcal{C}, \mathcal{D}, \mathcal{E}$ are Voronoi vertices and the segments $\overline{\mathcal{V}_1\mathcal{A}}$, and the arc $\widehat{\mathcal{BC}}$ are examples of Voronoi edges.

Proposition 3.4. *Let P be a polygon. Then $M(P) \subseteq \mathcal{VD}(P)$.*

Proof. Consider a point $x \in M(P)$, then x is a center of a maximal circle inscribed in P. Each maximal circle in P is tangent to at least two points on the boundary of P, i.e., x is equidistant to at least two different sites. Thus $x \in \mathcal{VD}(P)$. □

From the Proposition 3.4 and the definition of dominance we can also conclude that the medial axis is a union of straight line segments and parabolic arcs.

Theorem 3.2. *Let P be a simple polygon. Consider the set $E_r(P)$ of internal Voronoi edges incident to reflex vertices. Then,*

$$M(P) = \mathcal{VD}(P) - E_r(P). \tag{3.8}$$

Proof. The Voronoi diagram of a polygon P consists of edges that are incident to convex vertices, edges incident to reflex vertices and others that are not incident to any vertex. Let us suppose that x is on a Voronoi edge that is incident to a convex

vertex e_i, then x is on a bisector of segments e_{i-1} and e_{i+1} adjacent to e_i. Therefore, there exists a maximal disk in P centered at x. That is, $x \in M(P)$.

Next, suppose that x is on an edge that is not incident to any vertex of P. Then it is equidistant to two non-adjacent sites of the polygon and belongs to two Voronoi regions generated by these sites. This means that its minimum distance to the boundary is attained once in each site, consequently, $x \in M(X)$.

Finally, consider x that is only on an edge that is incident to a reflex vertex e_i. Furthermore, consider the disk centered at x with the radius $d(x, e_i)$. This disk is not maximal. Indeed, it is tangent on the polygon in just one point e_i and moving the center a bit a way from e_i along that incident edge and keeping the tangent point we get a disk that contains the previous disk. This means $x \notin M(X)$. □

For the convex case since there are no reflex vertices we get the following simplified statement.

Corollary 3.1. *If P is a simple convex polygon then,*

$$M(P) = \mathcal{VD}(P). \tag{3.9}$$

Suppose that a polygon P is not simple, that is, it contains holes in its internal region. We assume that the boundary of the hole is a polygon P'. Furthermore, we suppose that P' is strictly enclosed in the internal region of P. The region of interest will be the one bounded by ∂P and $\partial P'$ and let us denote it by $P \cap \overline{P'}^c$.

Theorem 3.3. *Let P be a non-simple polygon and $E_r(P \cap \overline{P'}^c)$ denote the set of internal Voronoi edges incident to a reflex vertex of $P \cap \overline{P'}^c$. Then,*

$$M(P) = \mathcal{VD}(P \cap \overline{P'}^c) - E_r(P \cap \overline{P'}^c). \tag{3.10}$$

The proof of this theorem is analogous to that of Theorem 3.2.

3.3. Truncated medial axis

To solve the original problem presented in Chapter 1, we can not use milling cutters of arbitrarily small radius, since each milling cutter is of some fixed radius. This is the reason why we will introduce the concept of truncated medial axis, which we are then going to use to find the reachable region in a polygon. The reachable region in a polygon P, is the set of points of this polygon that can be covered by disks of some fixed radius $s > 0$ contained in P, and we will denote by R_s.

Definition 3.4. *Given a disk of fixed radius s, we define a truncated medial axis, $M_s(P)$, of a polygon P to be the set of points in the medial axis that are centers of maximal disks with radius greater or equal to s.*

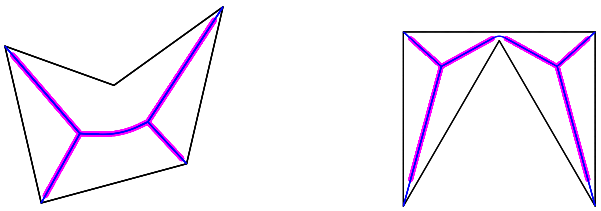

(a) (b)

Figure 3.9: The blue lines are the original medial axes and the magenta lines are the truncated medial axes for each polygon in which they are contained.

In Figure 3.9 we have depicted in magenta the truncated medial axes for each polygon whereas the original medial axes are in blue. We aim to find the reachable region. Thus, we consider the following theorem.

Theorem 3.4. *The region of a polygon that can be reached by a milling cutter of radius s is*

$$R_s = \bigcup_{x \in M_s(P)} B_{r_{\max}}(x).$$

Proof. If a point is covered by a disk of radius s, then it is covered by some maximal disk of radius greater or equal to s. On the other hand, any disk of radius greater or equal to s can be covered by disks of radius s. □

An example of a reachable region in a polygon is shown in Figure 3.10. The red area is the reachable region for the corresponding polygon. Notice that gaps on the reachable region correspond to truncated parts of the medial axis.

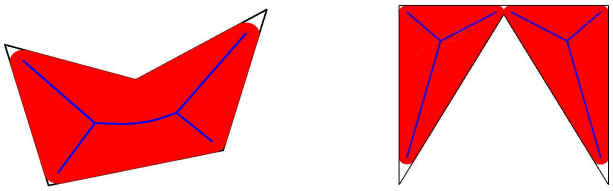

(a) (b)

Figure 3.10: The red area is the region in the respective polygon that can be reached by a milling cutter of some fixed radius.

Thus, with this technique we can identify in each section that is created when the additive process is interrupted the reachable region, hence finding the area that can be reached by the milling cutter for the corresponding slice.

***Observation* 3.1.** *The truncated medial axis does not need to be connected. In Figure 3.10b the image shows a disconnected truncated medial axis corresponding to connected reachable region.*

3.4. Algorithms

There are several efficient algorithms for computing the medial axis. These algorithms can be generally classified in two classes: *continuous* methods and *semi-continuous* methods. In the continuous methods, also called exact methods, a continuous shape is known and the exact medial axis is extracted from the full boundary, for instance, by using generalized Voronoi diagrams. In the *semi-continuous* methods the boundary is approximated by a sample of points which are then used to compute an approximated medial axis. For more details about algorithms for computing the medial axis methods see [14, 30]. For the purposes of this work we will focus on the semi-continuous methods, due to their flexibility and ease of implementation. They will be covered in detail in Section 3.5. In this section, for the sake of completeness we will provide a brief idea of the exact approaches.

Determining the medial axis with exact methods is only feasible for some geometrical shapes. A general class of shapes for which it is theoretically possible to compute the medial axis exactly are the *semi-algebraic sets* [32]. These sets are unions of the sets of solutions of finite systems of polynomial equations and inequalities. It can be seen that the medial axis of such a set is itself semi-algebraic and can be computed with tools from theoretical computational algebra, see [2]. These

algorithms are however not implementable in the real world and in practice only algorithms for more restricted shapes are available.

A first approach to compute the medial axis is to generalize the divide and conquer algorithm introduced in Section 2.2 to compute the classic Voronoi diagram to more general shapes. This can be done efficiently for polygons or regions bounded by straight line segments and arcs of circles, (see [13]). We can in this way obtain a $\mathcal{O}(n \log n)$ accuracy. We can then make use of Theorem 3.3 to compute the medial axis. These algorithms are however typically hard to implement and not stable.

A second, more stable approach, is based on domain decomposition. It works for shapes bounded by circular arcs and spline curves, and it is based on the following decomposition theorem proven by Choi [7].

Theorem 3.5. *Let X be a compact body whose boundary comprises circular arcs, spline curves and D be a maximal disk for X with center x. Then, if $X_1, X_2, \ldots, X_\alpha$ are connected components of $X \setminus D$, then*

$$M(X) = \bigcup_{i=1}^{\alpha} M(A_i \cup D), \tag{3.11}$$

$$\{x\} = \bigcap_{i=1}^{\alpha} M(A_i \cap D). \tag{3.12}$$

Using this result, a divide and conquer algorithm can be implemented until a finite number of basic cases is reached. This is more stable and easier to implement than the Voronoi based algorithm but it has a worst case complexity of $\mathcal{O}(n^{\frac{3}{2}})$. However in practical instances it is often the case that $\mathcal{O}(n \log n)$ can be achieved, and for more about this approach see [1, 3].

3.5. Medial axis approximation

In this section we review the semi-continuous methods based on the Voronoi diagrams. We discuss some basic theory that sustains the correctness of the approximation following [27], and exploit the theory of the Voronoi diagrams of a set of points that was treated in Section 2.1. Note that the boundary of a planar continuous shape can be approximated by a set of equally spaced points lying on that boundary. This set of equally spaced points is called sample or sampling of that boundary and will formally be defined later. Computing the Voronoi diagram of this sample we get that the Voronoi vertices inside the shape converge to an inner approximation of

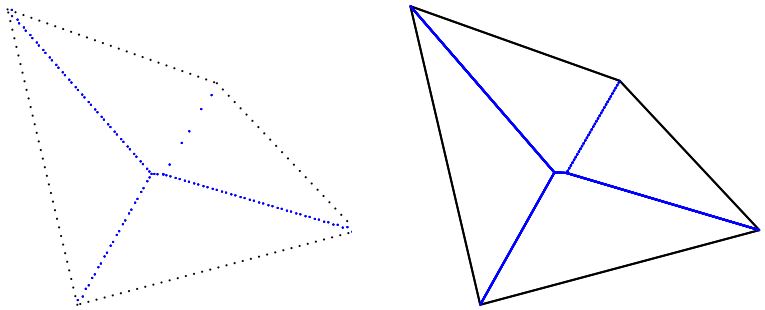

(a) (b)

Figure 3.11: Approximation of the medial axis by Voronoi vertices.

the medial axis of this shape, in this section we give the proof of this statement but only for polygons. In Figure 3.11a, the blue points are Voronoi vertices and as their density increases we can see that they tend to approximate the medial axis. This approximation of the medial axis may not recover it in its entirety. This can be true even if we restrict ourselves to the polygonal case. In Figure 3.11b we can see an example of a polygon where the approximation works while in Figure 3.13c we can see one where it does not .

To analyse the convergence of the semi-continuous methods we need to introduce some topological tools. Let us denote by H the set of the closed sets of $\mathbb{R}^2$ for the usual topology. We can endow H with a topology $\mathcal{T}$, the hit or miss topology, generated by the neighborhoods

$$\{F \in H : F \cap K = \emptyset,\ F \cap G_i \neq \emptyset\}$$

where K is a compact set and G_i, $i = 1, 2, \ldots, k$ is a finite family of open sets in $\mathbb{R}^2$. With this topology H is compact, Hausdorff and separable.

In terms of the convergence of sequences of closed sets, $\mathcal{T}$ can be interpreted as follows.

Property 3.1. *A sequence $\{S_i\}_{i\in\mathbb{N}}$ of closed sets converges towards S if and only if the following two criteria are simultaneously verified:*

1. *For all $x \in S$, there exists $x_i \in S_i$ such that x_i converges towards x as i goes to infinity.*

2. *Let $\{S_{i_k}\}_{i_k\in\mathbb{N}}$ be a subsequence of $\{S_i\}_{i\in\mathbb{N}}$ and $x_{i_k} \in S_{i_k}$. Then, if x_{i_k} converges towards x, $x \in S$.*

The pointwise convergence used is with the usual topology in $\mathbb{R}^2$. We proceed to define the lower and upper limits of sequences of closed sets.

Definition 3.5. *Let $\{S_i\}_{i\in\mathbb{N}}$ be a sequence of closed sets. Then*

1. *The* lower limit *of $\{S_i\}_{i\in\mathbb{N}}$ ($\liminf S_i$) is the set of all limits of sequences of points $x_i \in S_i$, that is, it is the greatest closed set verifying the criterion 1 of Property 3.1.*

2. *The* upper limit *of $\{S_i\}_{i\in\mathbb{N}}$ ($\limsup S_i$) is the set of all cluster points of sequences of points $x_i \in S_i$. It is the smallest closed set verifying the criterion 2 of Property 3.1.*

Particularly we have that S_i converges towards S if and only if $\limsup S_i = \liminf S_i$. These notations are important to understand the approximation results that are treated in this section. The convergence of a sequence of closed disks in H is characterized in the following property.

Property 3.2. *Let $\{B_i = B(x_i, r_i)\}_{i\in\mathbb{N}}$ be a convergent sequence of disks in H. Then, B_i converges towards $B(x, r)$ in H if and only if x_i converges to x and r_i converges to r. Otherwise, $\{B_i\}_{i\in\mathbb{N}}$ converges towards a generalized disk, i.e., either the empty set or a closed half-plane or $\mathbb{R}^2$.*

Definition 3.6. *A set S of points p_i, $i = 1, 2, \ldots, k$, on the boundary ∂X such that for every $x \in \partial X$ there is some p_i within a maximum distance of ρ from x is called a set of points of density ρ. We will usually call such a set a sample or sampling of X.*

An example of a sample set for a given polygon is shown in Figure 3.12.

Now consider a sequence of points $\{p_i\}_{i\in\mathbb{N}}$ sufficiently dense on the boundary of X. It is already known that the Delaunay triangulation of a point set S yields a tessellation with triangles of its convex hull and that the circumcircle of each triangle is centered at a Voronoi vertex and does not contain any other point of S, such circumcircles are called Delaunay disks, see Section 2.2.

The following proposition is one of the most important results that motivates the use of Voronoi diagrams to approximate the medial axis. It states that each sequence of centers of Delaunay disks converges to the center of a maximal disk, i.e, to a point of the medial axis of the polygonal compact body X.

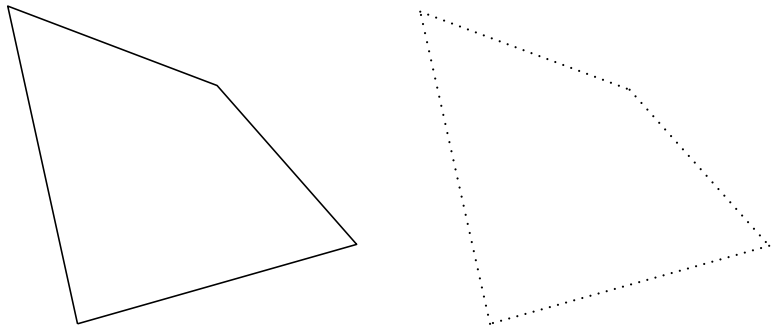

(a) (b)

Figure 3.12: The image in (b) shows a sample of the image in (a).

Proposition 3.5. *Let X be a polygon, S_i be a sequence of samples with density decreasing to zero and $\{B_i\}_{i\in\mathbb{N}}$ be a sequence of Delaunay disks. If B is a cluster point of B_i, then B if maximal in X or in $\overline{X^c}$. That is, if V_i is the set of Voronoi vertices associated to S_i then*

$$\lim_{i\longrightarrow\infty} \sup V_i \subseteq B_{max}(X).$$

Proof. Let $\{B_{i_k}\}$ be a subsequence of $\{B_i\}$ converging to B. It is known that $B_i = B(x_i, r_i)$ is a Delaunay disk and S_i is a sample of ∂X whose density is ρ_i, thus the disk $B(x_i, r_i - \rho_i)$ does not intercept the boundary ∂X. That means $B(x_i, r_i - \rho_i)$ is included into X or $\overline{X^c}$. We now consider a subsequence $\{B(x_{i_k}, r_{i_k} - \rho_{i_k})\}$ and we assume that it is totally contained in X or $\overline{X^c}$. It is clear by Property 3.2 that $\{B(x_{i_k}, r_{i_k} - \rho_{i_k})\}$ converges to B and since inclusions are preserved by taking limits we get that $B \subseteq X$ or $B \subseteq \overline{X^c}$. Now let us suppose that $B \subseteq X$ and let B' be such that $B \subseteq B' \subseteq X$, we will show that $B = B'$ which proves that B is maximal in X.

Denote by $(v^0_{i_k}, v^1_{i_k}, v^2_{i_k})$ the vertices of the triangle which B_{i_k} circumscribes. Extracting a subsequence, if necessary since the boundary of X is compact, we can assume that $(v^0_{i_k}, v^1_{i_k}, v^2_{i_k})$ converges to (v^0, v^1, v^2) in ∂X. They also belong by construction to B.

Now, suppose that two of these limits are different. Since they are on ∂X, B and B' that are contained in X, they must be on the boundary of B and B'. Given any two points any two disks that are tangent to them are uncomparable unless they are the same. Since $B \subseteq B'$ we have $B = B'$, thus B is maximal in X.

Finally, suppose that these limits are all equal to v, then v is a vertex of the

polygon X. If v is convex vertex then the radius of B' is zero and because $B \subseteq B'$ we get that $B = B'$. Note that v can not be a reflex vertex otherwise the sequence of Delaunay disks would not be in X. For $\overline{X^c}$ it is proven similarly. □

We have proven this proposition for a polygonal compact body X, however it is valid assuming some regularity on the boundary ∂X. One can be tempted to think that

$$\lim_{i \longrightarrow \infty} \inf V_i \supseteq B_{max}(X),$$

but, in general, this is not true. When the boundary of X is a polygonal line it is possible that the approximation of its medial axis through the Voronoi nodes of the Voronoi diagram of the samples fails, see Figure 3.13. In fact, it is also possible to assume some kind of regularity on the boundary of X that make this reverse inclusion hold, see [6, 27].

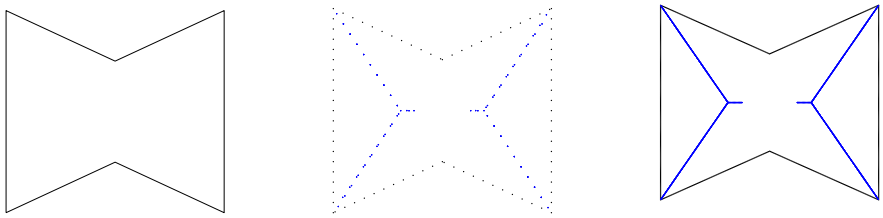

(a) (b) (c)

Figure 3.13: The image (a) is the original polygon. In image (b) we have the sample and Voronoi nodes or centers of Delaunay disks. The image (c) shows two non-connected curves that were found using the Voronoi nodes, but do not represent the medial axis.

Recall that if the polygon is connected its medial axis is also connected. In Figure 3.13 the line obtained with the Voronoi nodes is not connected, this is because no Delaunay disks can be found in some neighborhood of two opposite reflex vertices defined as in this polygon.

***Observation* 3.2.** *The curve obtained in the approximation presented in Figure 3.13 is not a truncated medial axis. The non-connectivity comes from the failure of the approximation.*

The situation reported in Figure 3.13 can be solved using the following result, that can be found in [20].

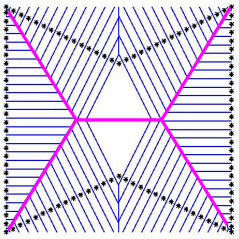

Figure 3.14: Approximation of medial axis using Voronoi edges and nodes. The magenta line approximates the original medial axis.

Theorem 3.6. *Let P be a polygon and S_i a sample with density ρ_i converging to zero. The medial axis $M(P)$ is the limit of the edges and vertices of $\mathcal{VD}(S_i)$ that are entirely contained in P.*

We exemplify this theorem in Figure 3.14. After we have sampled the polygon we find the Voronoi diagram that is in blue. The Voronoi edges and nodes inside the polygon approximate the original medial axis for a chosen density ρ, thus, the line highlighted in magenta is the approximation of the original medial axis.

Summarizing this section, to approximate the medial axis we follow the following steps.

1. We sample the polygon boundary guaranteeing that the distance between two consecutive points is no bigger than some fixed ρ.

2. We construct the Voronoi diagram of the sample points.

3. We keep the edges and vertices of the Voronoi diagram that are contained in the original polygon and discard the remaining.

What we get is an approximation of the medial axis, obtained in $\mathcal{O}(\frac{n}{\rho}log(\frac{n}{\rho}))$ time, that tends to the medial axis as the space between sample points, ρ, gets closer to zero. To find the truncated medial axis we just need the radius s of the milling cutter to be used and then to remove the points in the medial axis associated to the maximal disks with the radius less than s. For every vertex of the Voronoi diagram, checking if the maximal disk associated to it has radius less than s is very quick, and if that is the case we discard the vertex and the edges adjoining it. The only other thing to check is the edges that come from reflex vertices of P, such as the longer

edge in Figure 3.14. These tend to be longer than the other edges, since they will not be broken in pieces by the discretization, and can have both vertices respecting the radius property while some middle points do not. A fast way to study these edges is to check only for edges with length above a certain tolerance threshold, verify if they are formed by reflex vertices and, if so, look at the vertices of the polygon that generate them and see the distance between them. If it is larger than $2s$, the entire edge is kept, if it is lower, some quick computation can determine where the edge should be cut, and what portion remains. It can be shown that if we treat in this manner the results attained by the medial axis discrete approximation, we get an approximation to the truncated medial axis that will converge to the true truncated medial axis as ρ converges to zero as intended. For each ρ the corresponding approximate reachable region can easily be computed and will be an inner approximation to the true region. From the truncated medial axis one can immediately read the points on the boundary that will not be reached by the milling process, and hence get a measure on the attainable finishing quality for the slice. Other measures of quality, such as the area of the non-reachable surface, the topology of the reachable region (making sure that no crevice or hole is unreachable) can easily be implemented.

Chapter 4

Conclusions and considerations

The application of the medial axis technique gives us the reachable region for each section. We then are left with the question of how to go from applying this technique to each section to applying it to the original problem of determining where the additive problem should be interrupted. A first possible approach is to consider all fabrication slices, study each of them to determine the maximum tool diameter permitted in order to get an acceptable quality and also to find the maximum depth that such tool can reach. At each slice we obtain some stop restrictions that must be verified and we can find an optimal fabrication strategy to satisfy them all. Schematically, consider the object shown in Figure 4.1a and with its sections Figure 4.1b. We will study each section, as shown in Figure 4.1c, to scan for delicate details with our automatic procedure.

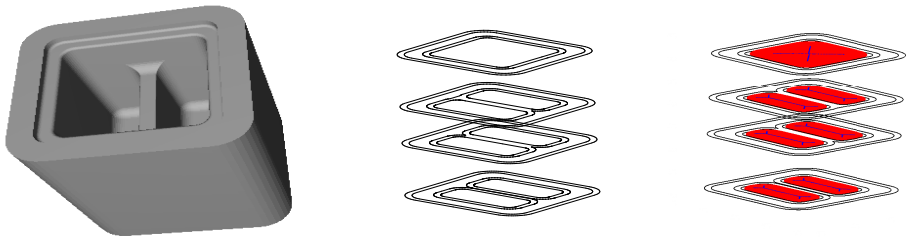

(a) (b) (c)

Figure 4.1: The image (a) is the object to be produced. In image (b) we have some sections of the object and in image (c) the red area represent some reachable regions for each section

There are however some simplifications that can be made, due to the framework we are considering. Since moulds need to be monotonous (meaning that the sections of the solid decrease in size when the height increases, without the creation of overhangs) one section being reached means all the above sections are reached, unless there is some change in the topology of the section (shallower details appear at certain heights). This allows us to not study every section but only those where there

are interesting changes in the topology, something that can also be easily detected by the use of medial axis. Some future work to be developed is the possibility of the desired finishing quality to be specified a priori by an operator and differ for different parts of the piece. Another point where improvements need to be introduced is on the handling of spherical drills, necessary to satisfactorily drill edges that are not vertical. However it is our belief that the properties of the medial axis make it again a perfect tool for handling these cases, possibly even by dealing with the 3-dimensional case by the direct use of the 3-dimensional structure of the medial axis of a polyhedron. In conclusion, in this work we propose the use of the medial axis and a variation of it to quickly deal with questions of access of a drill to a given surface. This allows us to measure finishing quality or even feasibility, and use it to plane the interruptions for a hybrid additive and subtractive fabrication method.

Bibliography

[1] O. Aichholzer, W. Aigner, F. Aurenhammer, T. Hackl, B. Jüttler, and M. Rabl. Medial axis computation for planar free form shapes. *Computer-Aided Design*, 41(5):339–349, 2009.

[2] D. Attali, J. D. Boissonnat, and H. Edelsbrunner. Stability and computation of medial axes-a state-of-the-art report. In *Mathematical foundations of scientific visualization, computer graphics, and massive data exploration*, pages 109–125. Springer, 2009.

[3] F. Aurenhammer, R. Klein, and D. T. Lee. *Voronoi diagrams and Delaunay triangulations*, volume 8. World Scientific, 2013.

[4] C. Bauer and H. Bischof. Extracting curve skeletons from gray value images for virtual endoscopy. In *International Workshop on Medical Imaging and Virtual Reality*, pages 393–402. Springer Berlin Heidelberg, 2008.

[5] H. Blum. A transformation for extracting descriptors of shape. *W. W. Dunn, Proc. Symp. Models for the Perception of Speech and Visual Form*, pages 362–380, 1967.

[6] J. W. Brandt. Convergence and continuity criteria for discrete approximations of the continuous planar skeleton. *CVGIP: Image Understanding*, 59(1):116–124, 1994.

[7] H. I. Choi, S. W. Choi, and H. P. Moon. Mathematical theory of medial axis transform. *Pacific journal of mathematics*, 181(1):57–88, 1997.

[8] N. D Cornea, D. Silver, and P. Min. Curve-skeleton properties, applications, and algorithms. *IEEE Transactions on visualization and computer graphics*, 13(3):530–548, 2007.

[9] J. C. de B. Dinis. *Construção e edição de diagramas de Voronoi na esfera*. PhD thesis, Universidade Nova de Lisboa, 2013.

[10] M. de Berg, O. Cheong, M. van Kreveld, and M. Overmars. *Computational Geometry: Algorithms and Applications*. Springer Science & Business Media, 2008.

[11] M. E. B. F. Gaspar. Sobre estratégias e métodos de optmização para pavimentar o interior de curvas planas fechadas através de trajetórias de traço contínuo. Master's thesis, Instituto Politécnico de Leiria, 2011.

[12] C. Gold and M. Dakowicz. Terrain modelling based on contours and slopes. In *Advances in Spatial Data Handling*, pages 95–107. Springer, 2002.

[13] M. Held. Vroni: An engineering approach to the reliable and efficient computation of voronoi diagrams of points and line segments. *Computational Geometry*, 18(2):95–123, 2001.

[14] F. Karimipour and M. Ghandehari. Voronoi-based medial axis approximation from samples: issues and solutions. In *Transactions on Computational Science XX: Special Issue on Voronoi Diagrams and Their Applications*, pages 138–157. Springer Berlin Heidelberg, 2013.

[15] I. Kloog and B. A. Portnov. Detecting the association between children health and lead exposure using voronoi polygon rezoning. In *Geography Research Forum*, volume 32, pages 46–61, 2016.

[16] J. C. Latombe. *Robot Motion Planning*, volume 124 of *The Springer International Series in Engineering and Computer Science*. Springer US, 1 edition, 1991.

[17] D. T. Lee and R. L. Drysdale III. Generalization of voronoi diagrams in the plane. *SIAM Journal on Computing*, 10(1):73–87, 1981.

[18] D.T. Lee. Medial axis transformation of a planar shape. *IEEE Transactions on pattern analysis and machine intelligence*, 4(4):363–369, 1982.

[19] G. Matheron. *Quelques propriétés topologiques du squelette*. Centre de géostatistique et de morphologie mathématique, 1978.

[20] S. N. Meshkat and C. M. Sakkas. Voronoi diagram for multiply-connected polygonal domains ii: Implementation and application. *IBM Journal of Research and Development*, 31(3):373–381, 1987.

[21] R Ogniewicz and M. Ilg. Voronoi skeletons: Theory and applications. In *Computer Vision and Pattern Recognition*, pages 63–69. IEEE, 1992.

[22] A. Okabe, B. Boots, K. Sugihara, and S. N. Chiu. *Spatial tessellations: concepts and applications of Voronoi diagrams*, volume 501. John Wiley & Sons, 2009.

[23] J. O'Rourke. *Computational geometry in C*. Cambridge university press, 1998.

[24] M. Petřek, P. Košinová, J. Koča, and M. Otyepka. Mole: a voronoi diagram-based explorer of molecular channels, pores, and tunnels. *Structure*, 15(11):1357–1363, 2007.

[25] F. Preparata and M. I. Shamos. *Computational geometry: an introduction*. 1985.

[26] F. P. Preparata and S. J. Hong. Convex hulls of finite sets of points in two and three dimensions. *Communications of the ACM*, 20(2):87–93, 1977.

[27] M. Schmitt. Some examples of algorithms analysis in computational geometry by means of mathematical morphological techniques. In *Geometry and robotics*, pages 225–246. Springer, 1989.

[28] J. Serra. *Image Analysis and Mathematical Morphology*, volume 1 of *Image Analysis and Mathematical Morphology Series*. Academic Press, 1984.

[29] M. I. Shamos. *Computational geometry*. PhD thesis, Yale University, 1978.

[30] V. Srinivasan and L. R. Nackman. Voronoi diagram for multiply-connected polygonal domains i: Algorithm. *IBM Journal of Research and Development*, 31(3):361–372, 1987.

[31] J. C Steuben, A. P. Iliopoulos, and J. G. Michopoulos. Implicit slicing for functionally tailored additive manufacturing. *Computer-Aided Design*, 77:107–119, 2016.

[32] L. L. Ta. An introduction to semi-algebraic sets (geometry on real closed field and its application to singularity theory). 2011.

[33] D. Thibault and C. M Gold. Terrain reconstruction from contours by skeleton construction. *GeoInformatica*, 4(4):349–373, 2000.